Comprehensive study of flow boiling modeling inside helical micro-finned tubes: Empirical, non-convex optimization and deep learning predictive models

Nima Irannezhad, Alexandre Stenger, Luisa Rossetto, Andrea Diani

International Journal of Heat and Mass Transfer 231 (2024) 125802

Contents lists available at ScienceDirect

International Journal of Heat and Mass Transfer

journal homepage: www.elsevier.com/locate/ijhmt

Comprehensive study of flow boiling modeling inside helical micro-finned tubes: Empirical, non-convex optimization and deep learning predictive models

Nima Irannezhad [a], Alexandre Stenger [b], Luisa Rossetto [a], Andrea Diani [a,*]

[a] Department of Industrial Engineering, University of Padova, Italy
[b] ICube - UMR 7357, Centre National de la Recherche Scientifique, Université de Strasbourg, France

ARTICLE INFO

Keywords:
Heat transfer coefficient
Frictional pressure drop
Flow boiling
Microfin tubes
Artificial intelligence
Machine learning

ABSTRACT

Over the past decades, the design of evaporators has experienced improvement due to accruing experimental and numerical research on flow boiling. For micro-finned geometries that are deemed promising in augmentation of thermal performance, several empirical models have been developed. Recently, to attain higher accuracies in modeling, authors also resorted to Artificial Intelligence (AI) techniques while encouraging their further investigations. In this case, a database comprised of 1358 experimental heat transfer coefficients (HTC) and frictional pressure drops per unit length (FPD) has been considered for a holistic assessment of flow boiling modeling methods. The wide range of geometric features within the database, which includes tubes with outside diameters from 3 mm to 7 mm, helps to acquire a more reliable evaluation of the models, since the flow boiling mechanism is strongly dependent on the geometric parameters.After evaluating three empirical models for the HTC, it was confirmed that, depending on the diameter, the flow boiling mechanism undergoes alterations pertinent to a balance between convective and nucleate boiling, and the models must be modified to account for these conditions.The mean average deviation (MAD) for the models was recorded to be 11.7 %, 22.2 %, and 21.5 % for Diani et al., Mehendale, and Tang and Li, respectively. Higher accuracies were obtained after modification of the empirical models, of which the most accurate one provides a MAD of 10.13 %. Moreover, by the implementation of a novel approach, for the first time, a power function correlation has been established among dimensionless parameters for a machine learning-powered model. The MAD of 10.9 % and 15.8 % was reported for the Nusselt number and the two-phase multiplier respectively. Artificial Neural Network (ANN) was also considered for modeling, and MADs of 4.6 % and 4.2 % were recorded for the Nusselt number and two-phase multiplier, respectively.

1. Introduction

In the current period, industrial and domestic units experience a rise of exigency regarding the installation of heat exchangers as a result of national and regional attempts to encourage the replacement of fossil fuel gas boilers. In the European zone, a novel study [1] suggests that member states have already implemented their national-level mandates regarding the phase-out of gas boilers, and similar legislations are to be expected by the EU for a clear establishment of objectives on a regional level. Another attempt [2] regarding the prediction of the potential market for heat pumps in the EU zone, estimates the cumulative heat capacity to be 23 GW in EU-28 while stating a growing potential for heat pump suppliers to be expected soon.

Considering such projections, the proper design of heat exchangers for flow boiling becomes a salient aspect in the future of heating systems. Fortunately, pertinent to the ubiquitous configuration of horizontal smooth tubes, scientific endeavors regarding flow boiling experienced growth in the last two decades as many empirical and numerical models were developed and suggested for the estimation of heat transfer coefficient (HTC) and frictional pressure drops (FPD), two imperative variables deemed decisive in sizing of heat exchangers. Some examples of such models are present in studies of [3–7]. Empirical models are inherently confined within their range of applicability and are mainly dependent on the testing conditions. One of the features that has a considerable impact on the modeling process is the tube geometry. In the context of smooth tubes, one study by Mahmoud and Karayiannis [8] perfectly captures the dependency of empirical models on geometrical

* Corresponding author at: Department of Industrial Engineering, University of Padova, Via Venezia 1 35131 Padova, ITALY.
E-mail address: andrea.diani@unipd.it (A. Diani).

https://doi.org/10.1016/j.ijheatmasstransfer.2024.125802
Received 22 February 2024; Received in revised form 1 May 2024; Accepted 30 May 2024
Available online 17 June 2024

Nomenclauture

Latin symbols

AR	aspect ratio (-)
Bo	Boiling number (-)
c	specific heat (J kg^{-1} K^{-1})
Co	confinement number (-)
D	diameter (m)
f	friction factor (-)
FPD	frictional pressure drop (Pa)
Fr	Froude number (-)
g	gravity (m s^{-2})
G	mass velocity (kg m^{-2} s^{-1})
h	fin height (m)
h_{LV}	latent heat of vaporization (J kg^{-1})
HF	heat flux (W m^{-2})
HTC	heat transfer coefficient (W m^{-2} K^{-1})
i	uncertainty
ID	inner diameter at fin tip (m)
J	superficial velocity (m s^{-1})
L	length (m)
M, MM	molar mass (kg $kmol^{-1}$)
$\dot{m}$	mass flow rate (kg s^{-1})
N, n_g	number of fins (-)
Nu	Nusselt number (-)
OD	outer diameter (mm)
P	pressure (Pa)
Pr	Prandtl number (-)
q	heat flow rate (W)
r	bubble radius (m)
Re	Reynolds number (-)
R_x	area enhancement ratio (-)
T	temperature (°C)
U	mean velocity (m s^{-1})
We	Weber number (-)
x	vapor quality (-)
X	Martinelli parameter (-)

Subscripts

crit	critical
exp	experimental
g	gas phase
i	at the fin tip
L	liquid phase
LO	liquid only
nb	nucleate boiling
onb	onset of nucleate boiling
p	at constant pressure
pred	predicted
r	at the fin root
red	reduced
sat	saturation
t	turbulent
v	vapor phase

Greek symbols

α	apex angle (°)
β	helix angle (°)
δ	liquid film thickness (m)
ε	void fraction (-)
λ	thermal conductivity (W m^{-1} K^{-1})
μ	dynamic viscosity (Pa s)
σ	surface tension (N m^{-1})
Φ^2	two-phase multiplier (-)

Abbreviations

ANN	artificial neural network
HT	heat transfer
MAD	mean absolute deviation
MRD	mean relative deviation

parameters. Juxtaposing their experimental results to 21 empirical models developed for macro and micro-sized tubes, they reported large variability in recorded mean absolute deviations (MADs) among the models. In addition to empirical models, recently machine and deep learning (ML and DL) methods are also utilized to construct models for the prediction of flow boiling inside tubes. These models are usually capable of superb predictions of HTC and FPD in the 10 % MAD range as the results demonstrated by [9,10]. However, difficulty in their implementation could be considered as a drawback compared with empirical modeling.

Alongside conventional tubes with smooth surfaces, finned structures are commonly used in industrial and domestic applications as well. While such tubes are available in various sizes, micro sizes are more prevalent as they possess a high heat transfer area-to-volume ratio while allowing lower refrigerant charges. Similar to conventional tubes, research is accruing regarding micro-finned tubes as well, as several examples can be found in open literature whose experimental campaigns are considerably diverse, including diverse test sections, refrigerants, and operating conditions. Chiou et al. [11] conducted experiments on the evaporation of R-22 and R-124 for mass fluxes of 100–400 kg m^{-2} s^{-1} and heat fluxes 5–20 kW m^{-2} inside a micro-finned tube of 8.96 mm inner diameter (ID) and recorded enhanced heat transfer coefficient by the magnitude of 1.5–3 times higher than a smooth tube of similar geometry. Similarly, for an 8.96 mm ID tube, Jiang et al. [12] tested four refrigerants (R22, R134a, R407C, and R410A) for mass fluxes and heat fluxes of 50, 250, and 450 kg m^{-2} s^{-1} and 5, 12.5 and 20 kW m^{-2}, respectively, and concluded several aspects to wit: the average of heat transfer coefficients is higher by a factor that is in the range of 1.69–1.86 compared to that of the smooth tube, and frictional pressure drops higher by 1.4. Another study [12] concentrates on an immiscible mixture of oil and refrigerant HFO-1234yf during boiling, inside a micro-finned tube of 7 mm outer diameter (OD), and states a more robust effect of the oil on HTC at lower saturation pressures. In smaller tube scales, Diani et al. [13] carried out an experimental campaign on a tube of 3.4 mm ID (at the fin tip) during flow boiling of R1234ze(E). In addition to measuring experimental data for HTC and FPD, the authors also suggested two novel correlations for their prediction that could suitably perform for micro-finned tubes. Yun et al. [14] throughout garnering experimental data from the open literature and implementation of non-dimensional expressions affecting the heat transfer phenomena inside micro-finned tubes, constructed an empirical model that is posited to be suitable for a variety of geometries, testing conditions, and refrigerant types. In a more holistic analysis of empirical models, Tang et al. [15] collected 2221 data points covering an expanded range of operating conditions (mass fluxes between 47 and 835 kg m^{-2} s^{-1}, heat fluxes between 3.9–85.2 kW m^{-2}, and tube diameters (at fin root) between 2.64–11.98 mm), assessed the accuracy of six promising models and proved that the model of Mehendale [16] with MAD of 25 % is the most accurate.

Artificial intelligence has been also employed in predictions of HTC inside micro-finned tubes and noticing the downside of such methodology regarding the lack of an explicit form of a correlation, Lin et al. [17] attempted to construct a correlation predicated on neural network architecture. Although this correlation is not comparable to the

empirical one in terms of simplicity of expression, it provides valuable insight into new deep learning models and their applications. Qiu et al. [18], collecting 2787 FPD data points, evaluated the accuracy of the machine learning algorithms and, while varying the input feature sets, concluded that most of the implemented algorithms recorded remarkable accuracies on the order of ten percent. The work of Chen et al. [19] is noteworthy as they conducted similar assessments on HTC as well. In general, with regard to micro-finned tubes, the literature is rich in experimental data with various operating conditions, data that are often used to evaluate the accuracy of predictive models. However, the empirical predictive models are rather unsatisfactory, particularly for tubes with smaller diameters, whose flow evaporation mechanism has often been reported to experience discrepancies in various experimental works [20–23,13]. Regarding predictive methods, ML and DL models while thoroughly covered in the context of flow condensation, are scarce regarding boiling. Furthermore, despite the impressive precision of such models that are commonly experienced in previous works, the inconvenience stemming from either the absence of an expression or the presence of an excessively complex one in models remains an unresolved aspect.

To respond to such shortcomings, in the following work, by garnering 1358 experimental data points for micro finned tubes having outer diameters (OD) of 3, 4, 5, and 7 mm from the Laboratory of Heat Transfer in MicroGeometries at the University of Padova, three empirical, two machine learning non-convex optimizations and two artificial neural network models were assessed and following contributions were made:

1. The empirical correlations of HTC were improved to account for the effect of fin geometry in small micro finned tubes.
2. With the help of a differential evolution optimization algorithm, for the first time, an explicit formula was derived for the prediction of HTC and FPD.
3. The non-convex optimization possesses an imperative potential by which the magnitude and interrelations between the input features and the outcome can be defined on an a priori basis, assisting in directing the optimization process in the right path that leads to the discovery of actual underlying thermo-physical phenomena.
4. Two models with outstanding accuracies were provided by artificial neural networks for the prediction of HTC and FPD.
5. The machine and deep learning models are further trustworthy as a result of a more improved learning process that is achieved by feeding a homogenous database in which experimental uncertainties are similar, methods of HTC evaluation are identical, and the same experimental facility is utilized for the tests.

It is worth noting that all experimental tests were mostly performed with low global warming potential (GWP) refrigerants for which high demand is expected as regulations [24] are already in place regarding the decommissioning of currently deployed ones.

2. Modelling

2.1. Database

1358 measured heat transfer coefficients (relative to flow inside the horizontal tube) and frictional pressure drop per unit length values were imported from references that can be found in Table 1, alongside experimental conditions and their experimental uncertainty that is evaluated based on the method of Kline and McClintock [25]. Every single datum is an averaged value considering vapor quality differences (inlet-outlet of test section) between 0.03 (low heat flux and high mass flux) and 0.4 (high heat flux and low mass flux). The definition of *HF* (heat flux), *G* mass flux is given by Eqs. (1) and 2.

$$HF = \dot{q}/(\pi D L_{HT}) \quad (1)$$

Table 1
Composition of database. *HF* is expressed in [kW m^{-2}], *G* in [kg m^{-2} s^{-1}].

Database	Operating Conditions	Experimental Uncertainty (mean)	Refrigerants	Geometry*
Liu et al. [26]	*HF*=10–50 *G*=50–400 T_{sat}=30 °C *x* = 0.1–0.99	i_{HF}=±2.2 % i_{HTC}=±4.1 % i_x=±0.028 i_{FPD}=5.2 %	R515B R1234ze(E)	7 mm OD 6.14 mm ID *N* = 50 *h* = 0.18 mm β=18° *α*=42° AR=0.02
Fig. A2 & [27]	*HF*=10–60 *G*=100–600 T_{sat}=30–40 °C	i_{HF}=±3.2 % i_{HTC}=±4.8 % i_x=±0.027 i_{FPD}=4.5 %	R515B R1234ze(E)	5 mm OD 4.28 mm ID *n* = 54 *h* = 0.15 mm β=30° *α*=12° AR=0.035
Diani and Rossetto [28]	*HF*=10–50 *G*=150–800 T_{sat}=20 °C *x* = 0.1–0.99	i_{HTC}=±3.7 % i_x=±0.028	R513A	4 mm OD 3.4 mm ID *n* = 40 *h* = 0.12 mm β=18° *α*=43° AR=0.035
Diani et al. [21]	*HF*=10–50 *G*=190–940 T_{sat}=30 °C *x* = 0.1–0.99	i_{HTC}=±3.7 % i_x=±0.026	R1234yf	4 mm OD 3.4 mm ID *n* = 40 *h* = 0.12 mm β=18° *α*=43° AR=0.035
Diani et al. [13]	*HF*=10–50 *G*=190–940 T_{sat}=30 °C *x* = 0.2–0.99	i_{HTC}=±2.7 % i_x=±0.032	R1234ze(E)	4 mm OD 3.4 mm ID *n* = 40 *h* = 0.12 mm β=18° *α*=43° AR=0.035
Diani et al. [21]	*HF*=10–50 *G*=190–755 T_{sat}=30 °C *x* = 0.2–0.99	i_{HTC}=±2.5 %	R134a	4 mm OD 3.4 mm ID *n* = 40 *h* = 0.12 mm β=18° *α*=43° AR=0.035
Diani et al. [20]	*HF*=10–50 *G*=375–940 T_{sat}=30 °C *x* = 0.2–0.95	i_{HTC}=±1.8 % i_x=±0.027	R1234yf	3 mm OD 2.4 mm ID *n* = 40 *h* = 0.12 mm β=7° *α*=42° AR=0.05
Diani et al. [22]	*HF*=10–50 *G*=375–940 T_{sat}=30 °C *x* = 0.2–0.95	i_{HTC}=±2.3 % i_x=±0.024	R1234ze(E)	3 mm OD 2.4 mm ID *n* = 40 *h* = 0.12 mm β=7° *α*=42° AR=0.05
Diani et al. [29]	*HF*=12–60 *G*=360–940 T_{sat}=30 °C *x* = 0.2–0.95	i_{HTC}=±2.3 % i_x=±0.024	R134a	3 mm OD 2.4 mm ID *n* = 40 *h* = 0.12 mm β=7°

(continued on next page)

Table 1 (*continued*)

Database	Operating Conditions	Experimental Uncertainty (mean)	Refrigerants	Geometry*
Diani et al. [30]	HF=12–60 G=200–800 T_{sat}=20 °C x = 0.1–0.99	i_{HTC}=±2.3 % i_x=±0.024	R513A	α=42° AR=0.05 3 mm OD 2.4 mm ID n = 40 h = 0.12 mm β=7° α=42° AR=0.05

* $AR = ID/h$.

$\dot{q}$ as the heat flow rate, D as the diameter that is evaluated based on the distance between the fin tips, and L_{HT} as the heat transfer length.

$$G = 4\dot{m}/(\pi D^2) \quad (2)$$

$\dot{m}$ as the mass flow rate.

As can be seen, a selection of pure HFOs and azeotropic mixtures of HFOs/HFCs with considerably low values of GWP are present in the experimental dataset. The experimental campaigns were all conducted at the Laboratory of Heat Transfer in MicroGeometries at the University of Padova. To provide a clear presentation of geometrical parameters namely helix angle (β), apex angle (α), fin height (h), and number of fins per tube circumference (n), Fig. 1 is given. The dimensionless numbers associated with each data point are evaluated and implemented for the construction of empirical and ML and DL models. The definition of such dimensionless numbers can be found in Table 2.

One consideration to which attention should be given in the assessment of Table 2, is regarding pressure gradients that have not been completely reported in all published sources, and therefore further information regarding the evaluation of the frictional pressure gradient component is given in Table A1. Moreover, it is important to note that, due to high experimental uncertainty, experimental points with saturation and wall temperature differences below 0.7 K have been ruled out from consideration in predictive models. The same applies to frictional pressure drop per unit length measurements with corresponding two-phase multiplier below 3 due to inherent difficulty in evaluating low values of pressure drop by differential pressure transducers at a reasonably high accuracy. Since the models developed and tested are

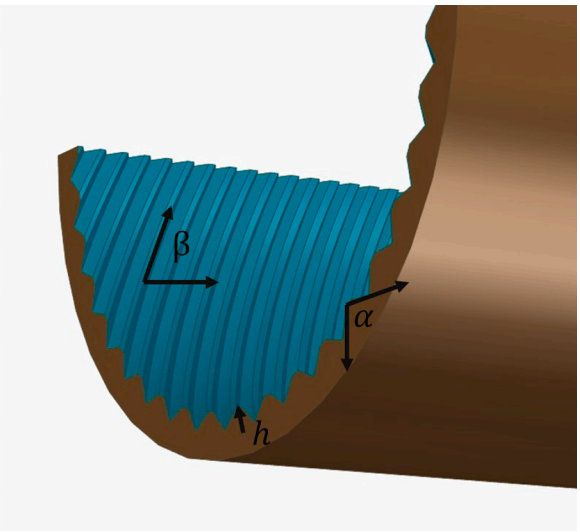

Fig. 1. Pictorial representation of geometrical features.

Table 2
Dimensionless parameters.

Parameter	Expression
Boiling number, Bo	$HF/(G \cdot h_{LV})$
Bond number, Bond	$(g \cdot \rho_L \cdot h \cdot \pi \cdot D)/(8 \cdot \sigma \cdot n)$
Confinement number, Co	$\sqrt{\frac{\sigma}{g(\rho_L - \rho_v)}}/D$
Martinelli parameter, X_{tt}	$\left(\frac{1-x}{x}\right)^{0.9}\left(\frac{\rho_v}{\rho_L}\right)^{0.5}\left(\frac{\mu_L}{\mu_v}\right)^{0.1}$
Liquid Reynolds number, Re_L	$G \cdot (1-x) \cdot D/\mu_L$
Vapor Reynolds number, Re_g	$G \cdot x \cdot D/\mu_v$
Liquid Prandtl number, Pr_L	$c_{p,L} \cdot \mu_L/\lambda_L$
Vapor Prandtl number, Pr_v	$c_{p,v} \cdot \mu_v/\lambda_V$
Liquid Weber number, We_{Ls}	$\rho_L \cdot U_{Ls}^2 \cdot D/\sigma$
Vapor Weber number, We_{vs}	$\rho_v \cdot U_{vs}^2 \cdot D/\sigma$
Liquid Froude number, Fr_L	$G^2 \cdot (1-x)^2/(\rho_L^2 \cdot g \cdot D)$
Vapor Froude number, Fr_v	$G^2 \cdot x^2/(\rho_v^2 \cdot g \cdot D)$
Area enhancement, R_x	$\left(\frac{2h \cdot n_g \cdot (1-\sin(\frac{\alpha}{2}))}{\pi \cdot D \cdot \cos(\frac{\alpha}{2}) + 1}\right)/\cos(\beta)$
Dimensionless gas velocity, J_G	$G \cdot x/(g \cdot D \cdot \rho_v(\rho_L - \rho_v))^{0.5}$

adequate for conditions where the dry-out phenomenon does not take place, data points after dry-out are also excluded from the database.

Fig. 2 is provided to further indicate the number of data points in each subcategory. As depicted, the data are evenly distributed between the type of geometries and refrigerants while reduced pressure points are mainly concentrated on the value of 0.16.

2.2. Empirical models and flow boiling mechanism

Flow vaporization inside tubes is commonly posited to depend on nucleate boiling and vaporization in two-phase forced convection; the sum of the two components gives the overall heat transfer coefficient. This assumption is a predicate for the formulation of many correlations [14–17,31–33]. Nucleate boiling refers to the formation of vapor bubbles and their expansion in the vicinity of the heat transfer surface while vaporization in two-phase forced convection happens when heat is transported by forced convection in the film from the wall to the liquid-vapor interface where evaporation takes place. One of the first attempts to model this mechanism was the correlation by Chen [34], using the equation of Forster and Zuber [35] for nucleate boiling. Several predictive models published later were mostly based on the same assumption of the summation of two components. For instance, Wellsandt et al. [32] in pursuit of defining a heat transfer model for herringbone finned tubes, proposed a modification to the convective boiling component to include area enlargement and turbulence inducive effect of fins. The focus of the current work is helical micro-finned tubes whose geometrical orientation results in significantly particular heat transfer and even frictional pressure drop mechanism compared to that of herringbone [32,36]. Several authors attempted to empirically modify the two aforementioned components. Hereby three HTC models that were centered over micro-finned tubes are considered for analysis. It should be acknowledged that all models considered in the current work apply to pre-dry-out regions.

Tang and Li [15] compiled 2221 data points covering a vast variety of operating conditions, geometries, and refrigerants. The database included mass fluxes in the range of 47–835 kg m^{-2} s^{-1}, heat fluxes between 3.9–85.2 kW m^{-2}, and tube diameters (based on fin root) from 2.6 to 11.98 mm. There is a considerably wide range of reduced pressures (0.05–0.61) in the dataset, which could be interpreted as a valuable advantage that helps to extend the predictive applicability of the model, since studies have recurrently shown reduced pressure's impact on nucleate boiling [37,38]. Essentially, the model is a modification of Cavallini et al. [33] as two alterations are imposed on convective and nucleate boiling expressions. The most noticeable aspect of the new correlation is where authors contend that as the tube diameter becomes

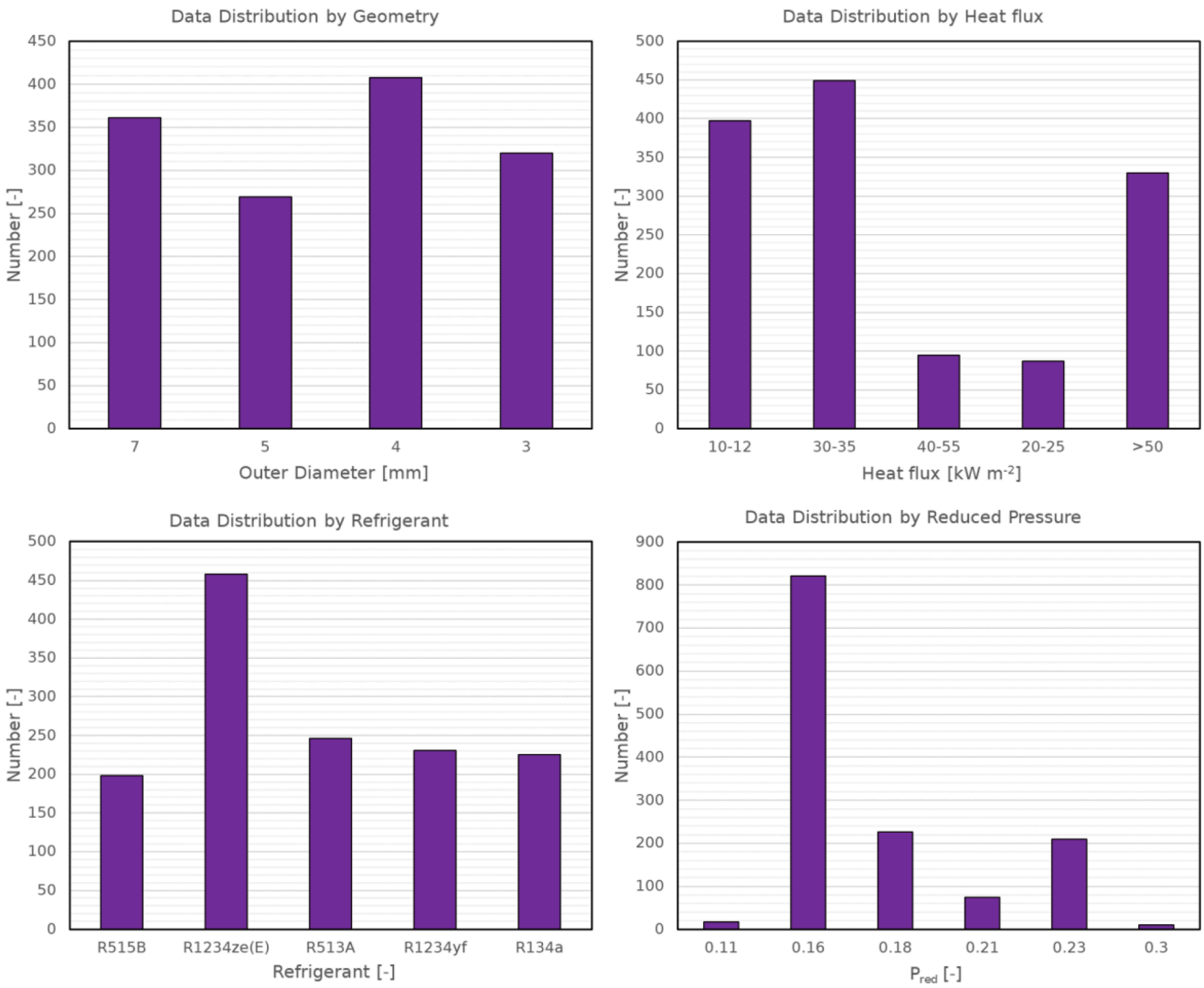

Fig. 2. Subcategorization of data points.

smaller, the presence of nucleate boiling components becomes diminutive to the degree of becoming negligible. Such postulation stems from the more robust nucleate suppression effect of tubes with smaller inner diameters as a result of a larger surface-to-volume ratio which results in significantly more predominant shear-stress force, mainly enhancing convective rather than nucleate boiling type. In evaluating the experimental results, the authors chose a threshold of 8 mm to consider this effect.

Diani et al. [13] developed their model on flow boiling experiments conducted on R1234ze(E) inside a micro-finned tube having an inner diameter of 3.4 mm. Their model similarly is a further improvement of Cavallini et al. [33] and advised to be applied to a tube of 3.4 mm ID between mass fluxes of 100–940 kg m^{-2} s^{-1}. Compared to the above-mentioned model [15], the nucleate boiling expression is rather attenuated, and different considerations are made for convective boiling.

Mehendale [16] by analyzing 2622 datapoints from a diverse background including pure and mixtures of HydroFluoroOlefins (HFOs) and HydroFluoroCarbons (HFCs), and CO_2, implemented a novel approach for the construction of an empirical model of the HTC. Such method is rather particularly exclusive as it does not follow the frequently adopted physical hypothesis of summation of nucleate and two-phase forced convection vaporization and possesses a rather influential mathematical aspect. In this case, the author argues that all dimensionless parameters that include physical, thermophysical features that are attested to impact the two-phase heat transfer coefficient inside micro-finned tubes by the literature, can all be considered to have a power function relation with the Nusselt number. Subsequently, the author proceeds to underscore 11 dimensionless parameters out of 38, as the most impactful ones with which a power function correlation with the Nusselt number is defined throughout the fitting process with the help of the database. The method by which the 11 parameters are identified is predicated on multitudinous steps in which the parameters with the lowest sum of errors are derived one by one.

The equations of enumerated models are provided in Table 3.

2.3. Model improvement considerations

As evident in the models presented in the last section, boiling inside helical micro-finned tubes has been posited to possess unique characteristics compared to smooth tubes. While models are strictly empirically built, flow boiling mechanisms were considered in the modification and adaptation of the general models. Knowledge of flow patterns greatly assists in the development of accurate models as the prevailing flow pattern is ultimately the decisive factor in heat transfer mechanisms. One study by [39] dedicated to flow visualization of evaporation inside helical micro-finned tubes, sheds light on the effect of fins. As visualizations attested, the helical grooves, in which the liquid phase flows due to surface tension forces, allow a more even distribution

Table 3
Correlations under consideration.

Model	Correlation
Tang and Li [15]	$h = h_{nb} + h_{cb}$ $h_{cb} = (\lambda_L / D_r)\mathrm{Nu}_{cv.p}\cdot R_x^{1.62}(\mathrm{Bond}\cdot\mathrm{Fr}_v)^t(0.01 / D_r)^{0.16}(100 / G)^{0.17}$ if $G < 500\,\mathrm{kg\,m^{-2}\,s^{-1}}$, $t = -0.1$ if $G > 500\,\mathrm{kg\,m^{-2}\,s^{-1}}$, $t = -0.18$ $\mathrm{Nu}_{cv.p} = [(1-x) + 2.63x(\rho_L/\rho_v)^{0.5}]^{0.8}(0.023\,\mathrm{Re}_{Lo}^{0.8}\,\mathrm{Pr}_L^{1/3})$ $h_{nb} = 55\mathrm{P}_{\mathrm{red}}^{0.12}(-\log_{10}\mathrm{P}_{\mathrm{red}})^{-0.55}M^{-0.5}HF_{eq}^{0.67}\mathrm{S}$ if $D_r \geq 8$ mm, $HF_{eq} = HF$ if $D_r < 8$ mm and $HF > HF_{onb}$, $HF_{eq} = HF - HF_{onb}$ if $D_r < 8$ mm and $HF < HF_{onb}$, $HF_{eq} = 0$ $HF_{onb} = \frac{2\sigma\cdot T_{sat}\cdot h_{cb}}{r_{crit}\cdot\rho_v\cdot h_{LV}}$ $r_{crit} = 0.38\cdot 10^{-6}$ $S = 1.36X_{tt}^{0.36}$
Diani et al. [13]	$h = h_{nb} + h_{cb}$ $h_{cb} = 1.465\,HTC_{LO}[1 + 1.128\,x^{0.8170}(\rho_L/\rho_v)^{0.3685}(\mu_L/\mu_v)^{0.2363}(1-\mu_v/\mu_L)^{2.144}\mathrm{Pr}_L^{-0.1}]\mathrm{R_x}^{2.14}(\mathrm{Bond}\cdot\mathrm{Fr})^{-0.15}(100/G)^{0.36}$ $HTC_{LO} = 0.023\,(\lambda_L / D_i)\mathrm{Re}_{Lo}^{0.8}\,\mathrm{Pr}_L^{1/3}$ $h_{nb} = 0.473\,HTC_{Cooper}\,S$ $S = 1.36X_{tt}^{0.36}$ $HTC_{Cooper} = 55P_{red}^{0.12}(-\log_{10}P_{red})^{-0.55}MM^{-0.5}HF^{0.67}$
Mehendale [16]	$\mathrm{Nu}_{\mathrm{Mehendale}} = 0.03771(\pi_{34}^{1.459})(\pi_{35}^{-1.139})(\pi_1^{0.6214})(\pi_{26}^{0.2249})(\pi_7^{0.2253})(\pi_{15}^{-0.1209})(\pi_{24}^{-0.6149})(\pi_{21}^{-0.04878})(\pi_6^{1.661})(\pi_8^{-0.04224})(\pi_{33}^{0.1121})$ $\pi_{34} = \frac{HF\cdot D_r}{h_{LV}\cdot\mu_L}$ $\pi_{35} = \frac{HF}{(h_{LV}^{1.5})(\rho_L-\rho_g)}$ $\pi_1 = \frac{(2h\cdot n)}{(\pi D_r)}\left(\sqrt{\frac{1}{\cos^2(\beta)} + \tan^2\left(\frac{\alpha}{2}\right)} - \tan\left(\frac{\alpha}{2}\right)\right) + 1$ $\pi_{24} = \frac{\rho_g\cdot\sigma\cdot D_r}{\mu_v^2}$ $\pi_{26} = \frac{D_r\cdot G^2\cdot x^2}{\rho_v\cdot\sigma}$ $\pi_7 = \frac{1-x}{x}$ $\pi_{21} = \frac{G^2\cdot D_r}{\rho_L\cdot\sigma}$ $\pi_6 = \frac{\rho_L-\rho_g}{\rho_l}$ $\pi_8 = \frac{MM}{2.016}$ $\pi_{33} = \frac{9.81(\rho_L-\rho_g)\cdot h\cdot D_r}{\sigma\cdot n}$ if $\mathrm{Re_L} < 2300$ $\pi_{15} = 4.364$ if $\mathrm{Re_L} > 2300$ $A = \left(2.457\cdot\log\left(\frac{\mathrm{Re_L}}{7}\right)^{0.9}\right)^{16}$ $B = \left(\frac{37530}{\mathrm{Re_L}}\right)^{16}$ $f_L = 8\left(\left(\frac{8}{\mathrm{Re}_L}\right)^{12} + \frac{1}{(A+B)^{1.5}}\right)^{\frac{1}{12}}$ $\pi_{15} = \frac{(f_L/8)\cdot(\mathrm{Re}_L - 1000)\,\mathrm{Pr}_L}{\left(1 + 12.7\left(\frac{f_L}{8}\right)^{0.5}(\mathrm{Pr}_L^{2/3} - 1)\right)}$

*$HF = q/(\pi\cdot D\cdot L)$

of liquid thickness along the circumference, facilitating the transition to annular flow patterns compared to smooth surfaces. Harboring a place for nucleation is also another function of finned surfaces that have been observed [40]. Lastly, the increase in heat transfer area is another aspect that directly contributes to the augmentation effect. Overall, finned surfaces bilaterally affect nucleate and convective boiling, however, it must be noted that the performance of the micro-finned tube is highly a function of operating conditions. For instance, in works of [40–43], it

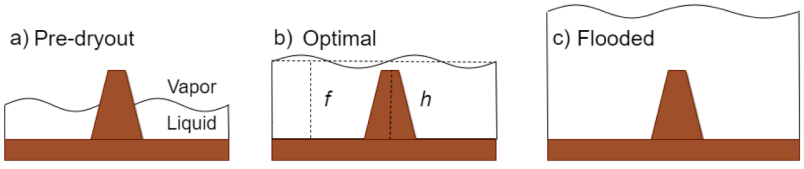

Fig. 3. Possible conditions present during the interaction between two-phase flow and fins.

has been argued that if liquid thickness becomes relatively smaller than fin height (as depicted in Fig. 3-a), the augmentation effect of micro-finned is attenuated and, if the liquid thickness is relatively higher than fin height (depicted in Fig. 3-c), the turbulence inducing effect of fins is diminished, rendering augmentation effects degraded. The authors further argue that the optimum design of a micro-finned tube should be such that the fin height and liquid thickness are comparable (depicted in Fig. 3-b) for most operating conditions. Having set forth these results regarding the influence of the fins, some caution must be taken in generalizing assumptions, since the mechanism of heat transfer within tubes is also highly dependent on diameter, as can be seen in the work of Kandlikar [44], in which the relative robustness of the various forces involved in two-phase flow was analyzed.

Overall, considering all the abovementioned aspects, the following dimensionless numbers are monitored within the database, in search of possible interrelations that could assist with the improvement of the models.

i. Confinement number (Co) which is commonly adopted by literary works (i.e. [44,45]) to analyze the effect of tube diameter has been considered.
ii. Boiling number Bo, which is widely utilized in the studies of boiling, could give insight into whether convective or nucleate boiling is the dominant mechanism.
iii. Weber number based on superficial vapor velocity We_{vs}, which evaluates the magnitude of shear stress forces.
iv. The ratio of liquid thickness to fin height (F) clarifies whether the fins are pre-dried, flooded, or under optimum conditions where the augmentation effect is the highest. Liquid thickness is calculated according to the method of Axelsson and Rouhani [46].

$$F = h/\delta_L \tag{3}$$

$$\delta_L = D\,(1-\varepsilon)/4 \tag{4}$$

$$\varepsilon = (x/\rho_v)\left[(1+0.12\,(1-x))\left(\frac{x}{\rho_v}+\frac{(1-x)}{\rho_L}\right)+\frac{1.18(1-x)\,(g\cdot\sigma(\rho_L-\rho_v))^{0.25}}{G\,\rho_L^{0.5}}\right] \tag{5}$$

2.4. Differential evolution modeling

Heat transfer coefficient and pressure drop have been commonly associated with the Nusselt number and two-phase multiplier as follows:

$$\mathrm{Nu} = HTC\cdot D_i/\lambda_L \tag{6}$$

$$\varnothing^2_{\mathrm{Lo}} = \mathrm{FPD}\Big/\frac{2\cdot f_{Lo}\cdot G^2\cdot L}{D_i\cdot\rho_L} \tag{7}$$

where f_{Lo} is the friction factor that is either evaluated with the help of the Moody chart.

In this case, the learning process is devised in a way that the relationship between the two dimensionless numbers (Nu, $\varnothing^2_{Lo}$) and the features are found. Such features are dimensionless numbers frequently implemented in flow boiling research over the course of the last two decades. The definition of these parameters was given in the aforementioned equations.

The explicit formula representing the relationship between the output (Nu – $\varnothing^2_{Lo}$) and the features are given in the form of a power function. For both outputs, this power function is in the following form:

$$\mathrm{Nu_{pred}} = \mathrm{R_x^{p_1}\cdot X_{tt}^{p_2}\cdot Re_g^{p_3}\cdot Re_L^{p_4}\cdot Pr_L^{p_5}\cdot Pr_v^{p_6}\cdot We_{Ls}^{p_7}\cdot We_{Vs}^{p_8}\cdot Fr_L^{p_9}\cdot Fr_v^{p_{10}}\cdot J_G^{p_{11}}\cdot Bo^{p_{12}}\cdot Bond^{p_{13}}\cdot P_{red}^{p_{14}}} \tag{8}$$

$$\varnothing^2_{\mathrm{Lo_{pred}}} = \mathrm{R_x^{p_1'}\cdot X_{tt}^{p_2'}\cdot Re_g^{p_3'}\cdot Re_L^{p_4'}\cdot Pr_L^{p_5'}\cdot Pr_v^{p_6'}\cdot We_{Ls}^{p_7'}\cdot We_{Vs}^{p_8'}\cdot Fr_L^{p_9'}\cdot Fr_v^{p_{10}'}\cdot J_G^{p_{11}'}\cdot Bo^{p_{12}'}\cdot Bond^{p_{13}'}\cdot P_{red}^{p_{14}'}} \tag{9}$$

with $p_1, p_2, \ldots, p_{14}$ the coefficients to optimize such that $\mathrm{Nu_{pred}}$ is related meaningfully with the input features (respectively $p_1', p_2', \ldots, p_{14}'$ for $\varnothing^2_{Lo_{pred}}$). We could directly optimize these coefficients to find a relationship. On the other hand, it is also possible to use prior knowledge to confine the coefficients ($p_1, p_2, \ldots, p_{14}$ and $p_1', p_2', \ldots, p_{14}'$) to be optimized regarding a specific range of values, to confine them to be solely positive or negative, as they are power factors.

Such definitions can be found in Table 4 for both HTC and FPD analyses. By assessing Table 4, it can be grasped that several features, whose relation to the corresponding output is not firmly established, are set to be decided by the machine learning model without limitation. Several other features are set to have either negative or positive power functions which are based upon multiple empirical evidence.

When those initial constraints were set, we used a Differential Evolution algorithm [47] to optimize this non-convex problem and find the optimal coefficients. 80 % of datapoints are reserved for the learning process and the remaining 20 % for testing.

The first step is to define a cost function that will be minimized by the algorithm.

For the sake of brevity, let $P = (p_1, p_2, \ldots, p_{14}) \in R^{14}$ be the vector of features associated with Nusselt number. Let n be the number of samples (i.e. the number of experimental observations). A specific sample (experimental observation) will be noted $\mathrm{Nu_{exp_i}}$ associated with its features ($\mathrm{X_{tt,i}}$, $\mathrm{Re_{l,i}}$, $\mathrm{Re_{g,i}}$, $\mathrm{We_{Ls,i}}$, *etc.*…) with $i \in [1,n]$. We define our cost function c in the following way:

$$c(P) = \frac{1}{n}\sum_{i=1}^{n}\left|\mathrm{Nu_{pred_i}} - \mathrm{Nu_{exp_i}}\right| \tag{10}$$

with $\mathrm{Nu_{pred_i}}$ defined on Eq. (8) and $\mathrm{Nu_{exp_i}}$ being the experimental observation associated. In other words, for each $\mathrm{Nu_{exp_i}}$ obtained experimentally, we compare it with the prediction from our power function parametrized by the coefficients $p_1, p_2, \ldots, p_{14}$, namely $\mathrm{Nu_{pred_i}}$. In the end, we mean all those comparisons to get the final cost associated with the current states of the parameter.

When the cost function c has been properly defined, we aim to

Table 4
Relations between features and the corresponding output.

Features	Associated Coefficient (*HTC*)	Associated Coefficient (*FPD*)	Coefficient sign (*HTC*)	Coefficient sign (*FPD*)
R_x	p_1	p_1'	+	+
X_{tt}	p_2	p_2'	–	–
Re_v	p_3	p_3'	+/-	+
Re_L	p_4	p_4'	+/-	+
Pr_L	p_5	p_5'	+	+
Pr_v	p_6	p_6'	+/-	+
We_{Ls}	p_7	p_7'	+/-	+
We_{vs}	p_8	p_8'	+	+
Fr_L	p_9	p_9'	+	+/-
Fr_v	p_{10}	p_{10}'	+	+/-
Jg	p_{11}	p_{11}'	+	+
Bo	p_{12}	p_{12}'	+/-	0
Bond	p_{13}	p_{13}'	+/-	–
P_{red}	p_{14}	p_{14}'	+/-	–

minimize it. In other words, we want to find the vector $P_{min} \in R^{14}$ for which c is the lowest so that the machine learning model will be as close as possible to the reality given by the experimental samples. To do so, we proceed as follows:

This algorithm first generates random vectors P1, P2, …, P20 $\in R^{14}$ that could be potential solutions to our optimization problems (of course, in the beginning, they are far away from the optimal P_{min}). Those 20 vectors will be called our "agents" and all together, they form our "population". After that, the way to find the best feature vector P_{min} is described below in Algorithm 1.

A similar procedure is undertaken for the two-phase multiplier and the results of both cases are given in Section 3.2.

2.5. Artificial neural network modeling

In the previous part, we correlated experimental features to the Nusselt number and the two-phase multiplier thanks to a physically meaningful power function. Nonetheless, it is possible to obtain better predictions through the help of Artificial Neural Networks (ANN). It is possible to get a nonlinear relationship between the desired output (in our case Nusselt number for example) and the input features (in our case X_{tt}, Re_L, Re_g, We_{Ls}, *etc.*…). This non-linear relationship is a function of the input features. However, this function is too complex to be explicitly given. Therefore, we call f_θ the function associated with the ANN, with θ the vectors containing the parameters of the ANN to optimize (as for the machine learning model, this is an optimization problem).

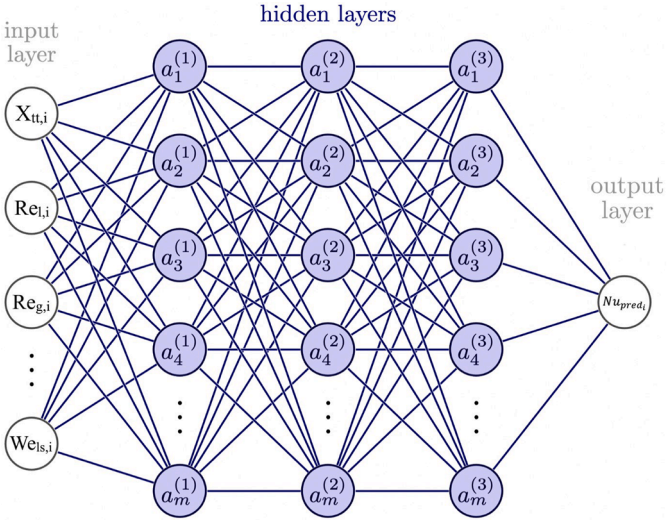

Fig. 4. Multilayer perceptron architecture.

Let n be the number of samples (i.e. the number of experimental observations). A specific sample (experimental observation) will be noted Nu_{exp_i} associated with its features ($X_{tt,i}$, $Re_{L,i}$, $Re_{g,i}$, $We_{Ls,i}$, …) with $i \in [1, n]$. This means in this case, $Nu_{pred_i} = f_\theta(X_{tt,i}, Re_{L,i}, Re_{g,i}, We_{Ls,i}, \ldots)$.

Similar to the Differential Evolution model, we need to define a cost function to minimize. We define our cost function c in the following way:

$$c(\boldsymbol{\theta}) = \frac{1}{n}\sum_{i=1}^{n}\left(Nu_{pred_i} - Nu_{exp_i}\right)^2 \tag{11}$$

$$c(\boldsymbol{\theta}) = \frac{1}{n}\sum_{i=1}^{n}\left(f_\theta\left(X_{tt,i}, Re_{L,i}, Re_{g,i},\ We_{Ls,i}, \ldots\right) - Nu_{exp_i}\right)^2 \tag{12}$$

After this cost function has been defined, the neural network (associated with the function f_θ) can be built. We opted for a fully connected feedforward neural network with 3 hidden layers, and ReLu [48] as an activation function. This is commonly called a Multilayer Perceptron (MLP). Each hidden layer has 256 neurons. The overview of the architecture can be found in Fig. 4. As said before, θ is the vector of parameters. The total number of parameters for this ANN is 135,681, which explains why it is not possible to give the explicit function.

Algorithm 1
Constrained Differential Evolution applied to our data.

1. Randomly generate 20 vectors $P_1, P_2, \ldots, P_{20} \in R^{14}$ (Our populations of Vectors with random coefficients inside)
2. Set(F = 0.7)(Mutation coefficient)
3. Set(C = 0.9)(Crossover coefficient)
4. Set(N_{iter} = 1000)(Number of iterations of the procedure)
5. while($N_{iter} \neq 0$):
a. For each(P_i) in ($P_1, P_2, \ldots, P_{20}$) do
i. Let ($P_i \in R^{14}$) be the current candidate
ii. Set ($y \leftarrow (0,0,\ldots,0) \in R^{14}$) be the concurrent candidate of (P_i)
iii. Pick randomly three agents (a, b, c) in the population of agents (P_1, P_2, …, P_{20})(Differents from (P_i))
iv. For (j) in range [1,14]):
−($r \sim U(0,1)$) (Generate a random real number between 0 and 1)
− If ($r < C$):
−(y[j] = a[j] + $F \cdot$ (b[j]-c[j])(In that case, proceed to the mutation)
Else
−(y[j] = Pi[j])(Otherwise, no mutation)
v. If (c(y) < c(P_i))(If the mutated candidate is better than the original one):
−(Pi ← y)(We substitute it in our population)
b. ($N_{iter} \leftarrow N_{iter} - 1$)
6. ($P_{min} = \min_i P_i, \forall_i \in [1, 20]$)(At the end of every mutation, we pick the best candidate over the 20)

More precisely, in Fig. 4, there are three layers. The input layer takes the 14 features of the experiment features ($X_{tt,i}$, $Re_{L,i}$, $Re_{g,i}$, $We_{Ls,i}$, *etc.* …). Then those features go through the hidden layers which are the core of the neural network. Each layer has $m = 256$ neurons.

More precisely, a neuron works as follows:

$$\alpha_i^j = \mathrm{ReLU}\left(\sum_{k=1}^{256} \theta_{ik}^j \cdot \alpha_k^{j-1} + \theta_i^{'j}\right) \tag{13}$$

where,

α_i^j is the output of neuron i in later j

ReLU is the Rectified Linear Unit activation function

θ_{ik}^j is the weight of the connection between neuron i in layer **j** and neuron k in later j-1

α_k^{j-1} is the output of neuron k in the previous layer (j-1)

$\theta_i^{'j}$ is the bias term for neuron i in layer j

Such that all together weights θ_{ik}^j and biases $\theta_i^{'j}$ makes our parameter vector θ that we aim to optimize.

The same procedure is then applied to the two-phase multiplier and the results of both cases are given in Section 3.2.

Similar to the machine learning model 80 % of datapoints were used as the learning set and the remaining 20 % as the testing set.

Table 5
Accuracy of models.

Model	Mean Absolute Deviation (MAD)*	Mean Relative Deviation (MRD)**
Diani et al. [13]	11.66 %	0.13 %
Mehendale [16]	22.21 %	4.59 %
Tang and Li [15]	21.54 %	−10.72 %

* $\mathrm{MAD} = \left[\sum_{i=1}^{n}\left|\frac{HTC_{model} - HTC_{exp}}{HTC_{exp}}\right|\right]/n.$

** $\mathrm{MRD} = \left[\sum_{i=1}^{n}\frac{(HTC_{model} - HTC_{exp})}{HTC_{exp}}\right]/n.$

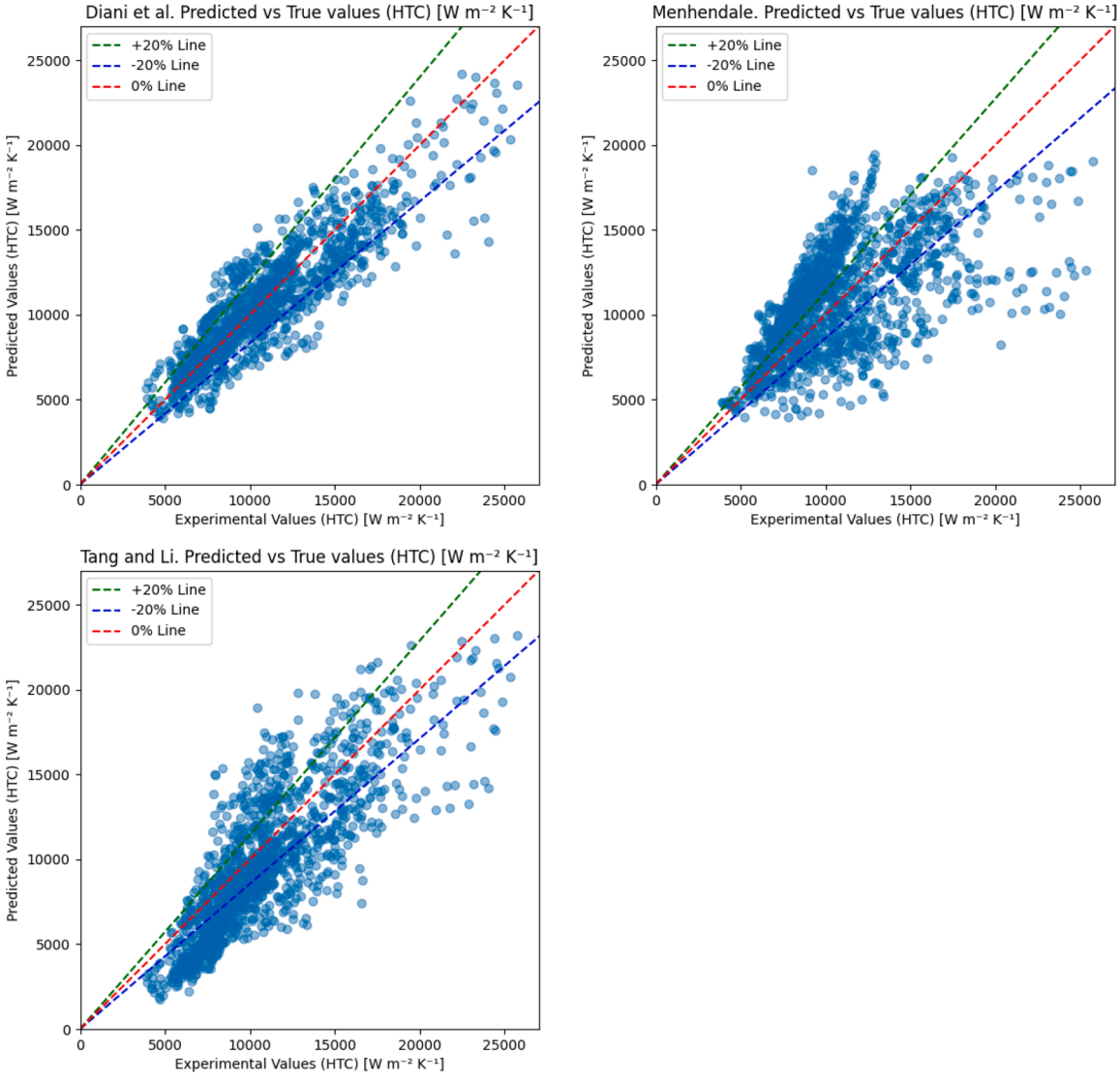

Fig. 5. Experimental and predicted values for heat transfer coefficient by Diani et al. [13], Mehendale [16], and Tang and Li [15].

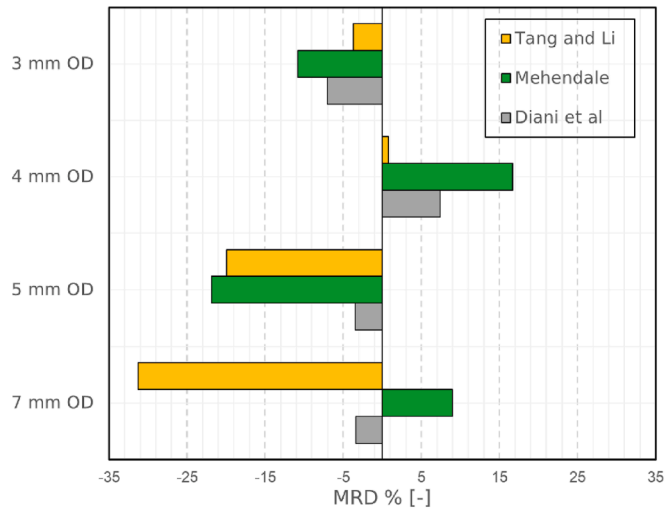

Fig. 6. Mean relative deviations of models for the subcategory of geometry.

3. Results

3.1. Empirical models for HTC

The deviation of data points predicted by the three models is depicted in Fig. 5. The model of Diani et al. [13] demonstrates the highest accuracy, followed by the model of Mehendale [16]. A common trait between the models is relatively attenuated accuracies at high values of heat transfer coefficient. The mean absolute deviation and mean relative deviation of the models are given in Table 5. The only model that underestimates the heat transfer coefficients on average is the one of Tang and Li [15]. Such underestimations are mostly associated with lower values of the heat transfer coefficient. Since the predictive accuracy of the models can be a function of tube geometry, Fig. 6 shows the MRD as a function of tube diameter. As is evident, by consensus, all models underestimate the HTC for the 5 mm and 3 mm outer diameter pipe, while overestimating the HTC for the 4 mm outer diameter pipe. It can be contended that peculiar characteristics of the 5 mm OD tube, such as the relatively high helix angle could contribute to such unanimous underestimations. Also the model of Tang and Li [15] underestimates the HTC for the largest diameter.

3.2. Proposed empirical models

As demonstrated in the last section, the predictive ability of the models worsens or improves for tubes of various sizes.

It was discovered that the model of Tang and Li [15] essentially underestimates the nucleate boiling element for the tube of 7 mm OD. Their hypothesis which imposed a reduction of nucleate boiling inside tubes with diameters lower than 8 mm OD due to suppression effects, is revealed to be fairly erroneous. Nucleate boiling is still comparable to convective boiling inside the tube of 7 mm OD and excluding the nucleate boiling component led to excessive underestimations, thus their model has been modified to impose limitations on nucleate boiling for diameters smaller than 5 mm OD. Furthermore, in the proposed new model, nucleated boiling is assumed to be zero for these tubes. Monitoring the ratio of liquid thickness to fin height, previously defined as (F), led to important results, as the model generally overestimates the heat transfer coefficient for values of F less than 0.8, an aspect that was previously thought to cause the phenomenon of pre-dryout, which was not considered in the construction of empirical models.

The model of Mehendale [16] mostly overestimates the heat transfer coefficients at high heat flux values, exclusively those higher than 30 kW m^{-2}. Moreover, since the model was built on a database that shared a limited amount of data for the inner diameters below 3 mm., it underestimates HTC at most operating conditions. After running multiple fitting attempts while concentrating on the alteration of coefficients regarding π_{34} and π_{35} as they are both associated with boiling numbers, a new model was proposed with an improved accuracy.

The model of Diani et al. [13], whose prediction is far superior to that of the previous two cases, has also undergone modifications. For the tube of 7 mm OD at low boiling numbers, which implies a relatively higher convective component during boiling, the model mostly underestimates the HTC. For low values of (F), which has been previously mentioned, the model similarly demonstrates overestimations.

A common aspect that emerged from the analysis of the models concerns the existence of a threshold delimiting the heat transfer mechanism that is particular. It has been previously argued that the boiling mechanism experiences discrepancies from macro to micro sizing for smooth tubes. The authors [49] in the literature review stated that the threshold between macro and micro has seen several proposals based on the confinement effect. In the current analysis, it has been discovered that once the confinement number reaches the value of 0.3 (almost entirely the data points of 3 mm OD) most models suffer from underestimations, as under such conditions the confinement effect alters the boiling mechanism where convective boiling component is deemed to be higher and more robust compared to the nucleate component, that has been suppressed. Almost all models can be ameliorated by intensifying the convective component at such conditions. The expressions of new models can be found in Table 6. Moreover, the deviation of the data points is provided in Fig. 7. The resulting accuracy of the modified models is given in the contents of Table 7.

In addition, Fig. 8 is provided to assess the accuracy of the models following the proposed changes. As can be seen, the models of Diani et al. [13] and Mehendale [16], demonstrate remarkably low MRD for tubes of 3, 4, and 7 mm OD. Another aspect present in the figure is that the model of Tang and Li [15] does not experience large underestimations after including the nucleate boiling component in the tube of 7 mm OD. It is evident that predictions for the tube of 5 mm OD are still experiencing high MRD, the reason for which could be traced to peculiar geometrical characteristics such as high fin density, and helix angle, compared to other cases. It is quite clear that, regardless of attempts at improvement, an empirical model is inherently confined to a specific operating condition in which it must be implemented. For this reason, artificial intelligence models will be explored in the next section to see if such limitations are solvable.

3.3. Differential evolution for HTC and FPD

Concluding the machine learning method, two models with explicit formulas were given (Eq. (14) and (15)). The accuracy of the models on the test set is depicted in Fig. 9. To assess the reliance of the model on tube geometry, data points are identified with their geometric characteristic. From what is evident in the figures, regarding the Nusselt number correlation, the model estimates the values mostly within $a \pm 20$ % range of deviation. In addition, one aspect of high importance concerning ML is the fact that, as opposed to most empirical models, the ML model although influenced, does not severely suffer from higher deviations at high values of Nusselt number that correspond to higher values of HTC. These large deviations at high HTC values are

Table 6
Newly proposed models.

Model	Correlation
Tang and Li [15] modified	if $F < 0.8$ $h = 0.95(h_{nb} + h_{cb})$ if $F \geq 0.8$ $h = h_{nb} + h_{cb}$ $h_{cb} = (\lambda / D_r)\mathrm{Nu_{cv.p}}\mathrm{Rx}^{1.62}(\mathrm{Bond}\cdot\mathrm{Fr_v})^{t}(0.01 / D_r)^{0.16}(100 / G)^{0.17}$ if $G < 500\,\mathrm{kg\,m^{-2}\,s^{-1}}$, $t = -0.1$ if $G > 500\,\mathrm{kg\,m^{-2}\,s^{-1}}$, $t = -0.18$ $\mathrm{Nu_{cv.p}} = [(1-x) + 2.63x(\rho_L/\rho_v)^{0.5}]^{0.8}(0.023\ \mathrm{Re_{Lo}^{0.795}\ Pr_L^{1/3}})$ $h_{nb} = 55\mathrm{P_{red}^{0.12}}(-\log_{10}\mathrm{P_{red}})^{-0.55}M^{-0.5}HF_{eq}^{0.67}\cdot\mathrm{S}$ if $D_r > 5$ mm, $HF_{eq} = HF$ if $D_r \leq 5$ mm, $HF_{eq} = 0$ $HF_{onb} = \dfrac{2\sigma\cdot T_{sat}\cdot h_{cb}}{r_{crit}\cdot\rho_v\cdot h_{LV}}$ $r_{crit} = 0.38\cdot 10^{-6}$ $S = 1.36X_{tt}^{0.36}$
Diani et al. [13] modified	if $F < 0.8$ $h = 0.95(h_{nb} + h_{cb})$ if $F \geq 0.8$ $h = h_{nb} + h_{cb}$ $h_{cb} = 1.465\ HTC_{LO}[1 + 1.128\ x^{0.8170}(\rho_L / \rho_v)^{0.3685}(\mu_L / \mu_v)^{0.2363}(1-\mu_v/\mu_L)^{2.144}\mathrm{Pr_L^{-0.1}}]R_x^{2.14}(\mathrm{Bond}\cdot\mathrm{Fr})^{-0.15}(90/G)^{0.36}$ if $\mathrm{Co} \geq 0.3$ $HTC_{LO} = 0.0265\ (\lambda_L / D_i)\mathrm{Re_{Lo}^{0.8}\ Pr_L^{1/3}}$ if $\mathrm{Co} < 0.15$ & $\mathrm{Bo} \leq 0.0006$ $HTC_{LO} = 0.027\ (\lambda_L / D_i)\mathrm{Re_{Lo}^{0.8}\ Pr_L^{1/3}}$ $0.15 \leq \mathrm{Co} < 0.3$ $HTC_{LO} = 0.023\ (\lambda_L / D_i)\mathrm{Re_{Lo}^{0.8}\ Pr_L^{1/3}}$ $h_{nb} = 0.478\ \mathrm{HTC_{Cooper}}\cdot\mathrm{S}$ $S = 1.36X_{tt}^{0.36}$ $HTC_{Cooper} = 55\mathrm{P_{red}^{0.12}}(-\log_{10}\mathrm{P_{red}})^{-0.55}M^{-0.5}HF^{0.67}$
Mehendale [16] modified	if $\mathrm{Co} \geq 0.3$ $\mathrm{Nu_{Mehendale}} = 0.03771(\pi_{34}^{1.355})\ (\pi_{35}^{-1.149})\ (\pi_1^{0.6214})\ (\pi_{26}^{0.2249})\ (\pi_7^{0.2253})\ (\pi_{15}^{-0.1209})\ (\pi_{24}^{-0.6149})\ (\pi_{21}^{-0.035})\ (\pi_6^{1.661})\ (\pi_8^{-0.04224})\ (\pi_{33}^{0.1121})$ if $\mathrm{Co} < 0.3$ $\mathrm{Nu_{Mehendale}} = 0.03771(\pi_{34}^{1.355})(\pi_{35}^{-1.149})\ (\pi_1^{0.6214})\ (\pi_{26}^{0.2249})\ (\pi_7^{0.2253})\ (\pi_{15}^{-0.1209})\ (\pi_{24}^{-0.6149})\ (\pi_{21}^{-0.075})\ (\pi_6^{1.661})\ (\pi_8^{-0.04224})\ (\pi_{33}^{0.1121})$ $\pi_{34} = \dfrac{HF\cdot D_r}{h_{LV}\cdot\mu_L}$ $\pi_{35} = \dfrac{HF}{h_{LV}^{1.5}\ (\rho_L - \rho_g)}$ $\pi_1 = \dfrac{(2h\cdot n)}{(\pi\cdot D_r)}\left(\sqrt{\dfrac{1}{\cos^2(\beta)} + \tan^2\left(\dfrac{\alpha}{2}\right)} - \tan\left(\dfrac{\alpha}{2}\right)\right) + 1$ $\pi_{24} = \dfrac{\rho_g\cdot\sigma\cdot D_r}{\mu_v^2}$ $\pi_{21} = \dfrac{G^2\cdot D_r}{\rho_L\cdot\sigma}$ $\pi_{26} = \dfrac{D_r\cdot G^2\cdot x^2}{\rho_v\cdot\sigma}$ $\pi_7 = \dfrac{1-x}{x}$ $\pi_6 = \dfrac{\rho_L - \rho_g}{\rho_L}$ $\pi_8 = \dfrac{MM}{2.016}$ $\pi_{33} = \dfrac{9.81\cdot(\rho_L - \rho_g)\cdot h\cdot D_r}{\sigma\cdot n}$ if $\mathrm{Re_L} < 2300$ $\pi_{15} = 4.364$ if $\mathrm{Re_L} > 2300$ $A = \left(2.457\cdot\log\left(\dfrac{\mathrm{Re_L}}{7}\right)^{0.9}\right)^{16}$ $B = \left(\dfrac{37530}{\mathrm{Re_L}}\right)^{16}$ $f_L = 8\left(\left(\dfrac{8}{\mathrm{Re_L}}\right)^{12} + \dfrac{1}{(A+B)^{1.5}}\right)^{\frac{1}{12}}$ $\pi_{15} = \dfrac{(f_L/8)\cdot(Re_L - 1000)\ \mathrm{Pr_L}}{\left(1 + 12.7\left(\dfrac{f_L}{8}\right)^{0.5}(\mathrm{Pr_L}^{2/3} - 1)\right)}$

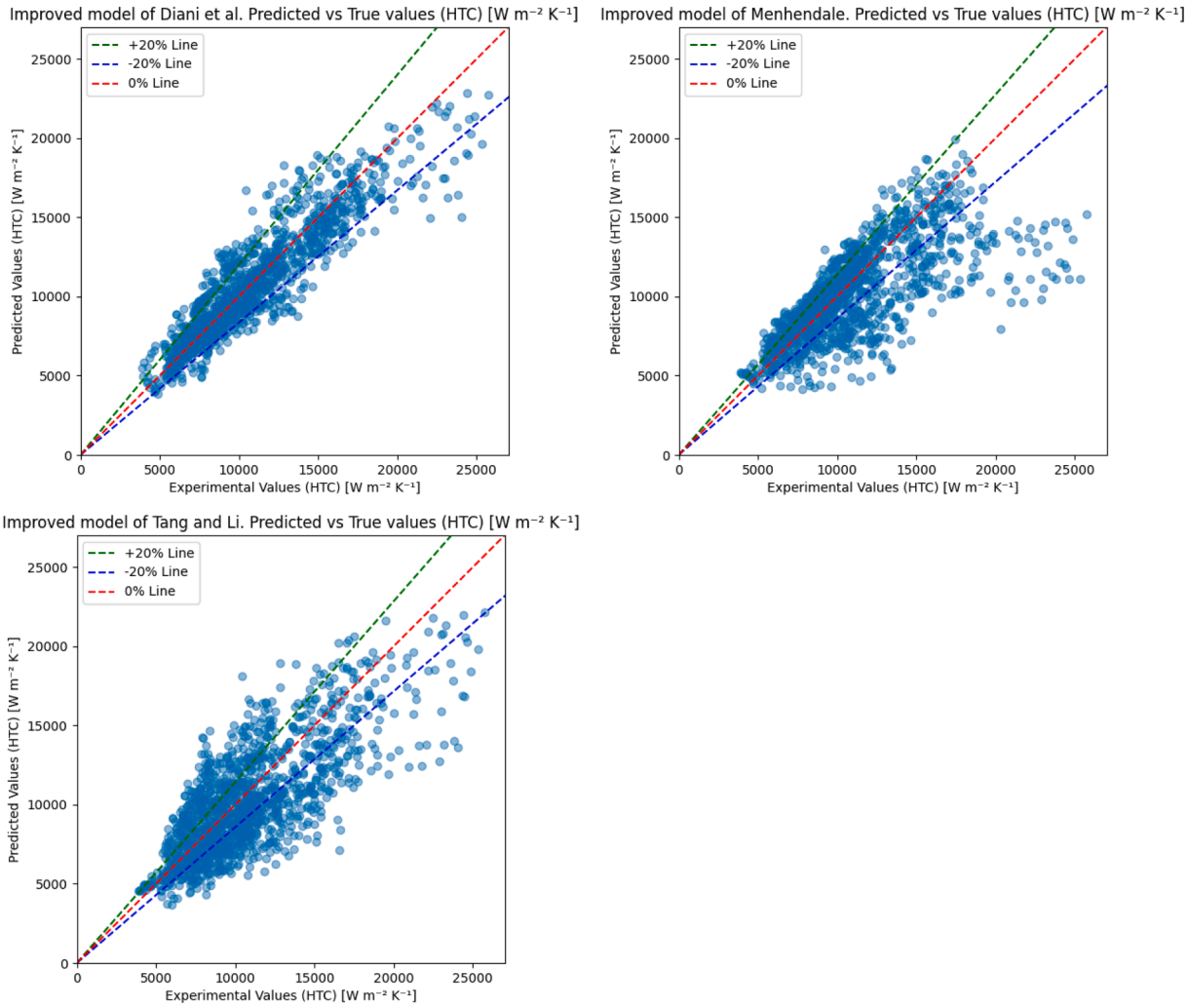

Fig. 7. Experimental and predicted values for heat transfer coefficient by improved Diani et al. [13], Mehendale [16], and Tang and Li [15] models.

Table 7
Accuracy of improved models.

Model	Mean Absolute Deviation (MAD)	Mean Relative Deviation (MRD)
Diani et al. [13]	10.13 %	0.70 %
Mehendale [16]	15.24 %	−2.94 %
Tang and Li [15]	19.22 %	−2.96 %

reoccurring within the literature regarding empirical modeling of HTC. For high vapor quality and high mass flux, the linearity of the relationship between vapor quality and HTC terminates and this model is capable to account for such occurrence. Hereby the ML model, contrary to the empirical models provides high accuracy even for high values of HTC. Moreover, in contrast to empirical models, ML models do not exhibit MAD variability with various diameters, as can be seen from the test set in Fig. 9.

Regarding the two-phase multiplier model, it can be said that there is a general tendency to overestimate for most values of frictional pressure drop per unit length. It could also be stated that the model is not necessarily superior to existing empirical models in open literature, as the model of [13] presents better accuracies, thus questioning ML models and the prevalence of claims regarding its superiority over empirical methods, as it may not always be the case. Lastly, the MAD on the testing set for the Nusselt number and the two-phase multiplier is 10.9 % and 15.8 % respectively.

3.4. Artificial neural network for HTC and FPD

The deviations of predictions made by the ANN model are depicted in Fig. 10. The MAD recorded for the Nusselt number, and the two-phase multiplier are 4.6 % and 4.2 % respectively. In consideration of Fig. 9, it can be seen that the predictions do not experience variability in the deviations recorded regardless of the value of the Nusselt number and

$$Nu = R_x^{1.6859} \cdot X_{tt}^{-0.0923} \cdot Re_v^{-0.6191} \cdot Re_L^{1.3197} \cdot Pr_L^{0.8813} \cdot Pr_v^{0.0727} \cdot We_{Ls}^{-0.8181} \cdot We_{Vs}^{0.2936} \cdot Fr_L^{0.1864} \cdot Fr_v^{0.0561} \cdot J_G^{0.0695} \cdot Bo^{0.0720} \cdot Bond^{0.4033} \cdot P_{red}^{0.4627} \quad (14)$$

$$\varnothing_{Lo}^2 = R_x^{0.3256} \cdot X_{tt}^{-0.4992} \cdot Re_v^{0.0054} \cdot Re_L^{0.0075} \cdot Pr_L^{0.9228} \cdot Pr_v^{0.0380} \cdot We_{Ls}^{0.0008} \cdot We_{Vs}^{0.0011} \cdot Fr_L^{0.1398} \cdot Fr_v^{-0.7128} \cdot J_G^{1.1073} \cdot Bond^{0.0026} \cdot P_{red}^{-1.4885} \quad (15)$$

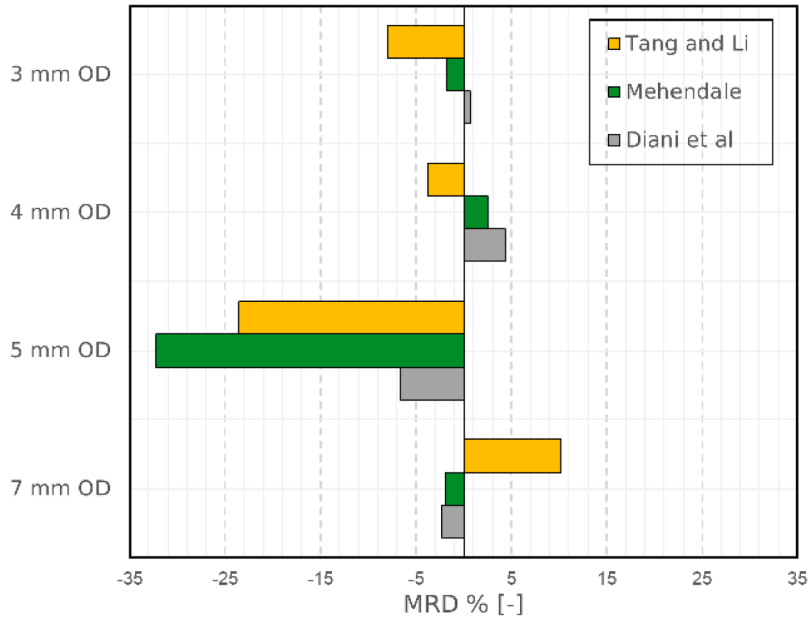

Fig. 8. Mean relative deviations of proposed models for the subcategory of geometry.

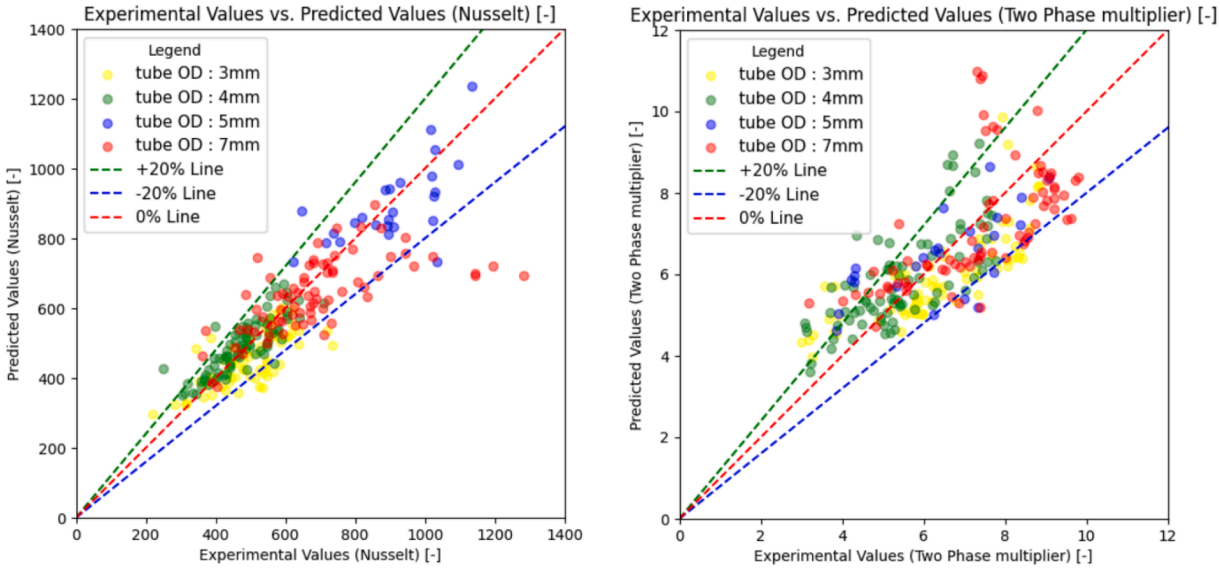

Fig. 9. Experimental and predicted values for Nusselt number and two-phase multiplier by ML model on 20 % of the database as a function of tube geometry.

the two-phase multiplier. As discussed in the previous section regarding the usual inaccuracy of models for high HTC values, higher HTC values here are even more excellently predicted compared to the ML model. The two-phase multiplier model is by far more accurate than the empirical and ML models. It is of high importance to recognize the interaction between features and outputs to shed light on the flow boiling mechanism. The ANN model predicts the HTC and FPD for all tube diameters with almost identical accuracy. However, as discussed, the black-box nature of ANN remains an impediment to the attainment of explicit correlations.

4. Discussions

It is rather evident that each modeling tool has its own merits and demerits. The empirical models offer fairly accurate predictions. However, they remain highly susceptible to error under various testing conditions. It was corroborated that geometry plays an indispensable role in the flow boiling heat transfer mechanism and thus it highly impacts the accuracy of models. Therefore, it becomes salient to distinguish a boundary condition in which the mechanism undergoes alterations. In a comparative analysis of the database, it was found that models require such boundary conditions to be set based on the confinement effect. Such effect was found to be quite fairly identifiable by expression of dimensionless confinement number (Co) whose utilization greatly assists in improving the accuracy of the predictions for those models based on summation of nucleate and convective boiling mechanisms as well as the ones built by power functions such as [16]. As previously hypothesized, the suppression effect causes the nucleate boiling component to become smaller compared to the convective component and according to the current assessment, the confinement number of 0.3 perfectly captures such phenomena. Most models should undergo modifications if the objective is to predict the heat transfer

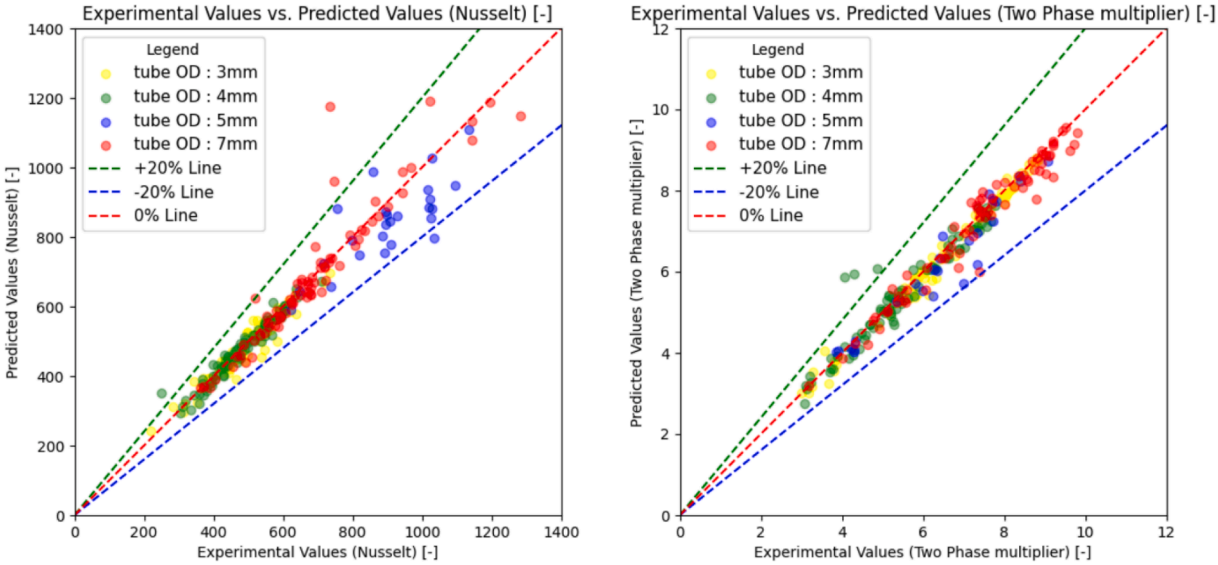

Fig. 10. Experimental and predicted values for Nusselt number and two-phase multiplier by ANN model on 20 % of the database as a function of tube geometry.

coefficient inside micro-finned tubes with confinement numbers close to the aforementioned threshold.

Artificial intelligence models, that are becoming widespread as multiple research papers are published [18,50–54], often fail at providing an expression that can be adopted without problems in real applications. Often such models require a large database on which the learning process must conclude before a novel model is built. Furthermore, such models offer little to no insight into the interrelations between features and the output. In the current paper, however, such aspect was resolved as the novel optimization methodology provided a correlation between features and the output in the form of a power function. Enforcing pre-established conditions (direct or inverse relation of features with the output) on the machine learning model not only led to higher accuracies but also resulted in the discovery of the degree of interactions between the features and the output.

As given, artificial neural network models offered exceptional accuracies despite their black-box nature in which the interrelations between features and output are opaque. This paper and many other examples of the application of ANN models in the field of heat transfer unanimously suggest superb accuracy in the adoption of such modeling methods.

Considering the recorded accuracies, it is suggested that the improved model of Diani et al. [13] for HTC and two machine and deep learning models for both HTC and FPD can be implemented for flow boiling inside micro-finned tubes with an applicability range of 3 to 7 mm OD, prior to the onset of dryout.

5. Conclusions

Compiling a flow boiling database comprised of four OD sizes of micro-finned tubes allowed a holistic assessment of flow boiling modeling. With the aid of such database, accuracies of three empirical models, Tang and Li [15], Diani et al. [13], and Mehendale [16], were evaluated. Aside from empirical modeling, machine and deep learning modeling methods were adopted and the following findings were reported:

1. It has been ascertained that the accuracy of the model of Tang and Li [15] and Mehendale [16] is highly dependent on tube diameter, where the former model results in the largest deviations for the smallest diameter of 3 mm OD (aspect ratio of 0.05). The same dependency on geometrical features, in a less pronounced way, applies to the model of Diani et al. [13] as well. MAD of the aforementioned models on the database was recorded to be 11.66 %, 22.21 %, and 21.54 % for Diani et al. [13], Mehendale [16], and Tang and Li [15] respectively.
2. To extend the applicability of empirical models to micro-finned tubes possessing a diameter of 3 mm OD, the empirical models should be modified to account for a more robust convective boiling component and an attenuated element of nucleate boiling due to the high suppression effect as a result of higher shear stress forces. Modifications are imposed for a confinement number of 0.3 or higher. Furthermore, monitoring aspects such as liquid thickness to fin height ratio and dimensionless parameters of boiling number and Weber number were deemed effective in the procedure of improvement of the models. The highest attainable accuracy by an empirical model by such modification was recorded to be 10.1 %.
3. For the first time in the context of flow boiling inside micro-finned tubes, the interplay between features and output was revealed in a machine learning model in the form of a power function correlation between dimensionless inputs and corresponding Nusselt number and two-phase multiplier. The recorded MADs on the testing set were 10.9 % and 15.8 % for HTC and FPD respectively.
4. A similar process was also adopted for Nusselt number and two-phase multiplier values by Artificial Neural Network by which superb accuracies were recorded. The MAD on the testing set was recorded to be 4.58 % and 4.15 % respectively.

Regarding the estimation of the heat transfer coefficient, even through improvement attempts, empirical models fail to provide uniform accuracy as variation in MAD is experienced for different tube diameters (especially that of 5 mm OD). Such aspect is not particularly surprising as the dependency of the accuracy of empirical models on test sections is experienced throughout the open literature. However, from the attained results of ML and DL modeling methods, it has been noticed that such dependency on tube geometry is attenuated, leading to the realization of the superiority of such modeling method over classical empirical modeling.

CRediT authorship contribution statement

Nima Irannezhad: Writing – original draft, Validation, Formal analysis, Data curation. **Alexandre Stenger:** Writing – original draft, Software, Methodology, Formal analysis. **Luisa Rossetto:** Writing –

review & editing, Supervision, Project administration, Conceptualization. **Andrea Diani:** Writing – review & editing, Supervision, Investigation, Conceptualization.

Declaration of competing interest

The authors declare that they have no known competing financial interests or personal relationships that could have appeared to influence the work reported in this paper.

Data availability

Data will be made available on request.

ANNEX

Table A1

Table A1
Evaluation of frictional pressure drop per unit of length.

Steps	Evaluation
Overall measured pressure gradient $\left(\frac{dP}{dZ}\right)_{total}$	measured by differential pressure transducer
Calculation of acceleration component* $\left(\frac{dP}{dZ}\right)_{a}$	$G^2 \frac{d}{dZ}\left[\frac{x^2}{\alpha\rho_v} + \frac{(1-x)^2}{(1-\alpha)\rho_L}\right]$
Frictional pressure gradient $\left(\frac{dP}{dZ}\right)_{f}$	$\left(\frac{dP}{dZ}\right)_{total} - \left(\frac{dP}{dZ}\right)_{a}$

* Void fraction calculated by the model of Rouhani and Axelsson [46].

Fig. A2

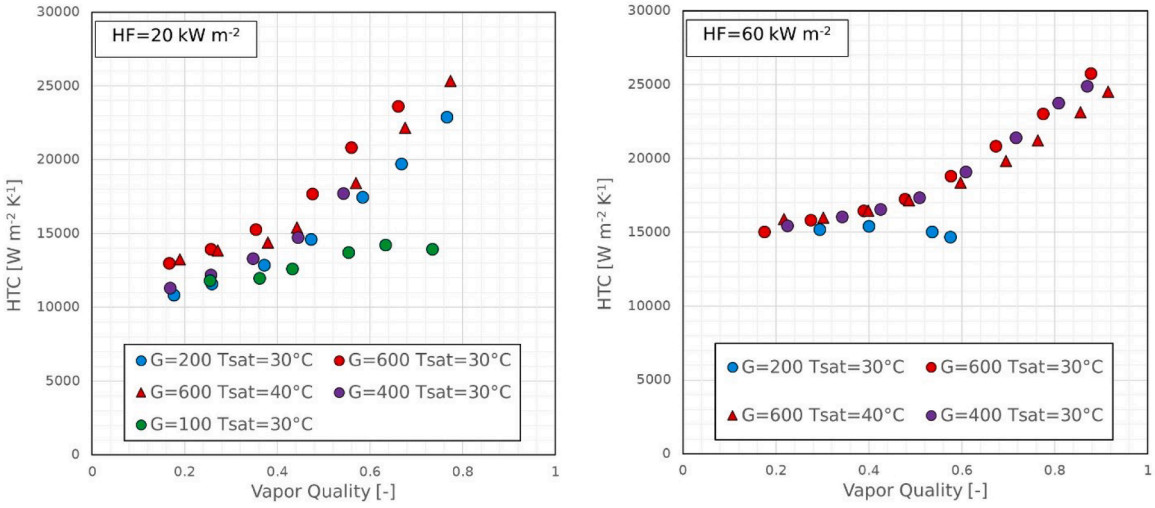

Fig. A2. *HTC* as a function of mass flux G [kg m^{-2} s^{-1}] and vapor quality (R1234ze(E) inside 5 mm OD microfin tube).

References

[1] S. Braungardt, B. Tezak, J. Rosenow, V. Bürger, Banning boilers: an analysis of existing regulations to phase out fossil fuel heating in the EU, Renew. Sustain. Energy Rev. 183 (2023) 113442.

[2] A. Marina, S. Spoelstra, H.A. Zondag, A.K. Wemmers, An estimation of the European industrial heat pump market potential, Renew. Sustain.Energy Rev. 139 (2021) 110545.

[3] X. Fang, A new correlation of flow boiling heat transfer coefficients based on R134a data, Int. J. Heat. Mass Transf. 66 (2013) 279–283, https://doi.org/10.1016/j.ijheatmasstransfer.2013.07.015.

[4] S.G. Kandlikar, A general correlation for saturated two-phase flow boiling heat transfer inside horizontal and vertical tubes, J. Heat. Transfer. 112 (1990) 219–228, https://doi.org/10.1115/1.2910348.

[5] W. Zhang, T. Hibiki, K. Mishima, Correlation for flow boiling heat transfer in mini-channels, Int. J. Heat. Mass Transf. 47 (2004) 5749–5763, https://doi.org/10.1016/j.ijheatmasstransfer.2004.07.034.

[6] W. Li, Z. Wu, A general correlation for evaporative heat transfer in micro/mini-channels, Int. J. Heat. Mass Transf. 53 (2010) 1778–1787, https://doi.org/10.1016/j.ijheatmasstransfer.2010.01.012.

[7] A. Berto, M. Azzolin, S. Bortolin, C. Guzzardi, D. Del Col, Measurements and modelling of R455A and R452B flow boiling heat transfer inside channels, Internat. J. Refrige. 120 (2020) 271–284, https://doi.org/10.1016/j.ijrefrig.2020.08.007.

[8] M.M. Mahmoud, T.G. Karayiannis, Heat transfer correlation for flow boiling in small to micro tubes, Int. J. Heat. Mass Transf. 66 (2013) 553–574, https://doi.org/10.1016/j.ijheatmasstransfer.2013.07.042.

[9] G. Zhu, T. Wen, D. Zhang, Machine learning based approach for the prediction of flow boiling/condensation heat transfer performance in mini channels with serrated fins, Int. J. Heat. Mass Transf. 166 (2021) 120783, https://doi.org/10.1016/j.ijheatmasstransfer.2020.120783.

[10] M.A. Moradkhani, S.H. Hosseini, M. Karami, Forecasting of saturated boiling heat transfer inside smooth helically coiled tubes using conventional and machine learning techniques, Internat. J. Refrige. 143 (2022) 78–93, https://doi.org/10.1016/j.ijrefrig.2022.06.036.

[11] C.B. Chiou, D.C. Lu, C.C. Chen, C.M. Chu, Heat transfer correlations of forced convective boiling for pure refrigerants in micro-fin tubes, Appl. Therm. Eng. 31 (2011) 820–826, https://doi.org/10.1016/j.applthermaleng.2010.10.031.
[12] G.B. Jiang, J.T. Tan, Q.X. Nian, S.C. Tang, W.Q. Tao, Experimental study of boiling heat transfer in smooth/micro-fin tubes of four refrigerants, Int. J. Heat. Mass Transf. 98 (2016) 631–642, https://doi.org/10.1016/j.ijheatmasstransfer.2016.03.024.
[13] A. Diani, S. Mancin, L. Rossetto, R1234ze(E) flow boiling inside a 3.4 mm ID microfin tube, Internat. J. Refrige. 47 (2014) 105–119, https://doi.org/10.1016/j.ijrefrig.2014.07.018.
[14] R. Yun, Y. Kim, K. Seo, H.Young Kim, A generalized correlation for evaporation heat transfer of refrigerants in micro-fin tubes, Int. J. Heat. Mass Transf. 45 (2002) 2003–2010, https://doi.org/10.1016/S0017-9310(01)00321-0.
[15] W. Tang, W. Li, A new heat transfer model for flow boiling of refrigerants in micro-fin tubes, Int. J. Heat. Mass Transf. 126 (2018) 1067–1078, https://doi.org/10.1016/j.ijheatmasstransfer.2018.06.066.
[16] S. Mehendale, A new heat transfer coefficient correlation for pure refrigerants and near-azeotropic refrigerant mixtures flow boiling within horizontal microfin tubes, Internat. J. Refrige. 86 (2018) 292–311, https://doi.org/10.1016/j.ijrefrig.2017.11.017.
[17] L. Lin, L. Gao, M.A. Kedzierski, Y. Hwang, A general model for flow boiling heat transfer in microfin tubes based on a new neural network architecture, Energy and AI 8 (2022) 100151, https://doi.org/10.1016/j.egyai.2022.100151.
[18] Y. Qiu, D. Garg, S.M. Kim, I. Mudawar, C.R. Kharangate, Machine learning algorithms to predict flow boiling pressure drop in mini/micro-channels based on universal consolidated data, Int. J. Heat. Mass Transf. 178 (2021) 121607, https://doi.org/10.1016/j.ijheatmasstransfer.2021.121607.
[19] B.L. Chen, T.F. Yang, U. Sajjad, H.M. Ali, W.M. Yan, Deep learning-based assessment of saturated flow boiling heat transfer and two-phase pressure drop for evaporating flow, Eng. Anal. Bound. Elem. 151 (2023) 519–537, https://doi.org/10.1016/j.enganabound.2023.03.016.
[20] A. Diani, A. Cavallini, L. Rossetto, R1234yf Flow boiling heat transfer inside a 2.4-mm microfin tube, Heat Transfer Eng. 38 (2017) 303–312, https://doi.org/10.1080/01457632.2016.1189260.
[21] A. Diani, S. Mancin, L. Rossetto, Flow boiling heat transfer of R1234yf inside a 3.4mm ID microfin tube, Exp. Therm. Fluid. Sci. 66 (2015) 127–136, https://doi.org/10.1016/j.expthermflusci.2015.03.019.
[22] A. Diani, S. Mancin, A. Cavallini, L. Rossetto, Experimental investigation of R1234ze(E) flow boiling inside a 2.4 mm ID horizontal microfin tube, Internat. J. Refrige. 69 (2016) 272–284, https://doi.org/10.1016/j.ijrefrig.2016.06.014.
[23] A. Padovan, D. Del Col, L. Rossetto, Experimental study on flow boiling of R134a and R410A in a horizontal microfin tube at high saturation temperatures, Appl. Therm. Eng. 31 (2011) 3814–3826, https://doi.org/10.1016/j.applthermaleng.2011.07.026.
[24] A. Mota-Babiloni, P. Makhnatch, Predictions of European refrigerants place on the market following F-gas regulation restrictions, Internat. J. Refrige. 127 (2021) 101–110.
[25] Describing uncertainties in single-sample experiments, Mech. Eng. 75 (1963) 3–8. https://cir.nii.ac.jp/crid/1572261549103675008.bib?lang=en (accessed January 6, 2024).
[26] Y. Liu, L. Rossetto, A. Diani, Flow boiling of R450A, R515B, and R1234ze (E) Inside a 7.0 mm OD microfin tube: experimental comparison and analysis of boiling mechanisms, Applied Sciences 12 (2022) 12450.
[27] A. Diani, Y. Liu, L. Rossetto, Flow boiling of r450a and r515b inside a 5.0 mm od microfin tube, in: International Heat Transfer Conference Digital Library, Begel House Inc., 2023.
[28] A. Diani, L. Rossetto, R513A flow boiling heat transfer inside horizontal smooth tube and microfin tube, Internat.J. Refrige. 107 (2019) 301–314, https://doi.org/10.1016/j.ijrefrig.2019.07.023.
[29] A. Diani, A. Cavallini, L. Rossetto, R134a flow boiling inside a 2.4 mm ID microfin tube, in: ASME ATI UIT 2015. Conference proceeding thermal energy systems: production, storage, utilization and the environment, Enzo Albano Editore di Albano V., 2015, pp. 1–7.
[30] A. Diani, L. Rossetto, Characteristics of R513A evaporation heat transfer inside small-diameter smooth and microfin tubes, Int. J. Heat. Mass Transf. 162 (2020) 120402, https://doi.org/10.1016/j.ijheatmasstransfer.2020.120402.
[31] K.E. Gungor, R.H.S. Winterton, A general correlation for flow boiling in tubes and annuli, Int. J. Heat. Mass Transf. 29 (1986) 351–358, https://doi.org/10.1016/0017-9310(86)90205-X.
[32] S. Wellsandt, L. Vamling, Prediction method for flow boiling heat transfer in a herringbone microfin tube, Internat. J. Refrige. 28 (2005) 912–920, https://doi.org/10.1016/j.ijrefrig.2005.01.009.
[33] A. Cavallini, D. Del Col, L. Rossetto, Flow boiling inside microfin tubes: prediction of the heat transfer coefficient [C], in: Proceedings of ECI International Conference on Boiling Heat Transfer. Spoleto, Italy, 2006.
[34] J.C. Chen, Correlation for boiling heat transfer to saturated fluids in convective flow, Industr. Eng. Chem. Process Design Develop. 5 (1966) 322–329.
[35] H.K. Forster, N. Zuber, Dynamics of vapor bubbles and boiling heat transfer, AIChE J. 1 (1955) 531–535, https://doi.org/10.1002/aic.690010425.
[36] A. Miyara, K. Nonaka, M. Taniguchi, Condensation heat transfer and flow pattern inside a herringbone-type micro-fin tube, Internat. J. Refrige. 23 (2000) 141–152, https://doi.org/10.1016/S0140-7007(99)00037-7.
[37] Z.Y. Bao, D.F. Fletcher, B.S. Haynes, Flow boiling heat transfer of Freon R11 and HCFC123 in narrow passages, Int. J. Heat. Mass Transf. 43 (2000) 3347–3358, https://doi.org/10.1016/S0017-9310(99)00379-8.
[38] K. Keniar, F. Mazzelli, S. Garimella, Experimental investigation of carbon dioxide flow boiling in a single microchannel, Int. J. Heat. Mass Transf. 159 (2020) 120100, https://doi.org/10.1016/j.ijheatmasstransfer.2020.120100.
[39] C.M. Yang, P. Hrnjak, Effect of helical micro-fins on two-phase flow behavior of R410A evaporating in horizontal round tubes obtained through visualization, Int. J. Heat. Mass Transf. 144 (2019) 118654, https://doi.org/10.1016/j.ijheatmasstransfer.2019.118654.
[40] R. Pastuszko, Pool boiling heat transfer on micro-fins with wire mesh – Experiments and heat flux prediction, Internat. J. Thermal Sci. 125 (2018) 197–209, https://doi.org/10.1016/j.ijthermalsci.2017.11.019.
[41] A. Muzzio, A. Niro, S. Arosio, Heat transfer and pressure drop during evaporation and condensation of R22 inside 9.52-mm OD microfin tubes of different geometries, J. Enhan. Heat Transfer 5 (1998).
[42] R. Yun, Y. Kim, K. Seo, H.Y. Kim, A generalized correlation for evaporation heat transfer of refrigerants in micro-fin tubes, Int. J. Heat. Mass Transf. 45 (2002) 2003–2010.
[43] N. Irannezhad, L. Rossetto, A. Diani, Flow condensation of low-GWP zeotropic mixtures inside 5 mm OD micro-finned tube, Appl. Sci. 14 (2024) 373, https://doi.org/10.3390/app14010373.
[44] S.G. Kandlikar, Scale effects on flow boiling heat transfer in microchannels: a fundamental perspective, Internat. J. Thermal Sci. 49 (2010) 1073–1085, https://doi.org/10.1016/j.ijthermalsci.2009.12.016.
[45] S. Kang, J.H. Seo, J. Lee, Effect of inner diameter on the confinement of two-phase closed thermosyphon, Internat. Commun. Heat Mass Transfer 147 (2023) 106997, https://doi.org/10.1016/j.icheatmasstransfer.2023.106997.
[46] S.Z. Rouhani, E. Axelsson, Calculation of void volume fraction in the subcooled and quality boiling regions, Int. J. Heat. Mass Transf. 13 (1970) 383–393.
[47] R. Storn, K. Price, Differential evolution – a simple and efficient heuristic for global optimization over continuous spaces, J. Global Optimiz. 11 (1997) 341–359, https://doi.org/10.1023/A:1008202821328.
[48] K. Fukushima, Cognitron: a self-organizing multilayered neural network, Biol. Cybern. 20 (1975) 121–136.
[49] C.B. Tibiriçá, G. Ribatski, Flow boiling in micro-scale channels – Synthesized literature review, Internat. J.Refrige. 36 (2013) 301–324, https://doi.org/10.1016/j.ijrefrig.2012.11.019.
[50] L. Zhou, D. Garg, Y. Qiu, S.M. Kim, I. Mudawar, C.R. Kharangate, Machine learning algorithms to predict flow condensation heat transfer coefficient in mini/micro-channel utilizing universal data, Int. J. Heat. Mass Transf. 162 (2020) 120351, https://doi.org/10.1016/j.ijheatmasstransfer.2020.120351.
[51] Y. Qiu, D. Garg, L. Zhou, C.R. Kharangate, S.M. Kim, I. Mudawar, An artificial neural network model to predict mini/micro-channels saturated flow boiling heat transfer coefficient based on universal consolidated data, Int. J. Heat. Mass Transf. 149 (2020) 119211, https://doi.org/10.1016/j.ijheatmasstransfer.2019.119211.
[52] M.T. Hughes, B.M. Fronk, S. Garimella, Universal condensation heat transfer and pressure drop model and the role of machine learning techniques to improve predictive capabilities, Int. J. Heat. Mass Transf. 179 (2021) 121712, https://doi.org/10.1016/j.ijheatmasstransfer.2021.121712.
[53] I. Mudawar, S.J. Darges, V.S. Devahdhanush, Prediction technique for flow boiling heat transfer and critical heat flux in both microgravity and Earth gravity via artificial neural networks (ANNs), Int. J. Heat. Mass Transf. 220 (2024) 124998, https://doi.org/10.1016/j.ijheatmasstransfer.2023.124998.
[54] E. Efatinasab, N. Irannezhad, M. Rampazzo, et al., Machine and deep learning driven models for the design of heat exchangers with micro-finned tubes, Energy AI 16 (2024) 100370, https://doi.org/10.1016/j.egyai.2024.100370.